Off-Axis Elastic Properties and the Effect of Extraframework Species on Structural Flexibility of the NAT-Type Zeolites: Simulations of Structure and Elastic Properties

Jennifer J. Williams, Christopher W. Smith, and Kenneth E. Evans*

School of Engineering, Computer Science and Mathematics, The University of Exeter, North Park Road, Exeter, EX4 4QF, U.K.

Zoe A. D. Lethbridge and Richard I. Walton*

Department of Chemistry, The University of Warwick, Coventry, CV4 7AL, UK

Received October 17, 2006. Revised Manuscript Received March 12, 2007

Simulations of the atomic structure and elastic constants of five zeolites with the NAT-type structure, namely, natrolite, mesolite, scolecite, metanatrolite, and ammonium-exchanged natrolite, using the CVFF force field implemented within Cerius^2, are presented. The validity of the simulation method is shown by the excellent agreement between simulated and experimental crystal data, including location of extraframework ions and water molecules, and for natrolite, the only zeolite studied here for which experimental studies of elasticity have been reported, the good agreement between the simulated and experimental elastic constants. For all materials, an off-axis analysis of the elastic constants reveals that the Poisson's ratios ν_{xy} and ν_{yx} become negative when stress is applied at 45° to the crystallographic axes. Further simulations of the elastic behavior of the materials under stress, using the molecular dynamics method of Parrinello and Rahman, reveal that the elastic behavior may be described by a "modified rotating squares" model. Here three-dimensional structural distortions are reduced to a two-dimensional model where square cross-section units of structure both rotate about their hinges and undergo change of dimension: the balance of these competing processes dictates the resulting Poisson's ratio and is highly dependent upon the direction along which stress is applied. We discuss the effect that various concentrations of extraframework cations and water have on the elastic properties of the NAT-type zeolites.

Introduction

An understanding of the elastic properties of silicate network structures has implications in diverse areas from geology to nanotechnology. This encompasses the study of dense silicate minerals, in particular, the perovskite $MgSiO_3$ and related phases, which are of importance in understanding the seismic properties of the Earth's crust,[1] through to the study of the structural flexibility of open-framework zeolite materials which is of relevance to characterizing their nanoscale, shape-selective ion-exchange, catalytic, and sorption properties.[2] Several of the silicate structures, as well as polymorphs of silica itself, have been characterized by the presence of "rigid unit modes" where local flexibility results from oxygen hinges linking corner-sharing, rigid tetrahedral silicate building units.[2,3] These considerations have then been used to explain properties of silicates such as negative thermal expansivity,[4] compressibility,[5] and ion-exchange selectivity.[2]

Simulations of the elastic properties of zeolites have predicted some unusual properties for some of the materials, which also may be accounted for by the presence of rigid unit modes, in particular, the presence of negative Poisson's ratios in certain crystallographic directions for a number of zeolite framework types, implying a counterintuitive lateral widening upon longitudinal stress (known as auxetic behavior).[6] The low-density silica polymorph α-cristobalite, in fact, is one of the few crystalline materials to have been shown experimentally to possess a bulk (aggregate) negative Poisson's ratio,[7] and this behavior has also been interpreted using a model in which the concerted rotation of rigid tetrahedral units about their linked corners is dominant over other structural distortions, leading to an opening out of the structure upon application of stress.[8,9] Materials possessing

* To whom correspondence should be addressed. E-mail: r.i.walton@warwick.ac.uk; k.e.evans@exeter.ac.uk.

(1) Yeganeh-Haeri, A. *Phys. Earth Planet. Inter.* **1994**, *87*, 111.
(2) Hammonds, K. D.; Heine, V.; Dove, M. T. *J. Phys. Chem. B* **1998**, *102*, 1759.
(3) Dove, M. T.; Trachenko, K. O.; Tucker, M. G.; Keen, D. A. Rigid Unit modes in Framework Structures: Theory, Experiment and Applications. In *Reviews in Mineralogy and Geochemistry*; Redfern, S. A. T., Carpenter, M. A., Eds.; Mineralogical Society of America: Washington D.C., 2000; Vol. 39, pp 1−33.
(4) Lightfoot, P.; Woodcock, D. A.; Maple, M. J.; Villaescusa, L. A.; Wright, P. A. *J. Mater. Chem.* **2001**, *11*, 212.
(5) Angel, R. J.; Ross, N. L.; Zhao, J. *Eur. J. Mineral.* **2005**, *17*, 193.
(6) Grima, J. N.; Jackson, R.; Alderson, A.; Evans, K. E. *Adv. Mater.* **2000**, *12*, 1912.
(7) Yeganeh-Haeri, A.; Weidner, D. J.; Parise, J. B. *Science* **1992**, *257*, 650.
(8) Alderson, A.; Evans, K. E. *Phys. Rev. Lett.* **2002**, *89*, 225503.
(9) Kimizuka, H.; Kaburaki, H.; Kogure, Y. *Phys. Rev. Lett.* **2000**, *84*, 5548.

10.1021/cm062473w CCC: $37.00
Published on Web 04/20/2007

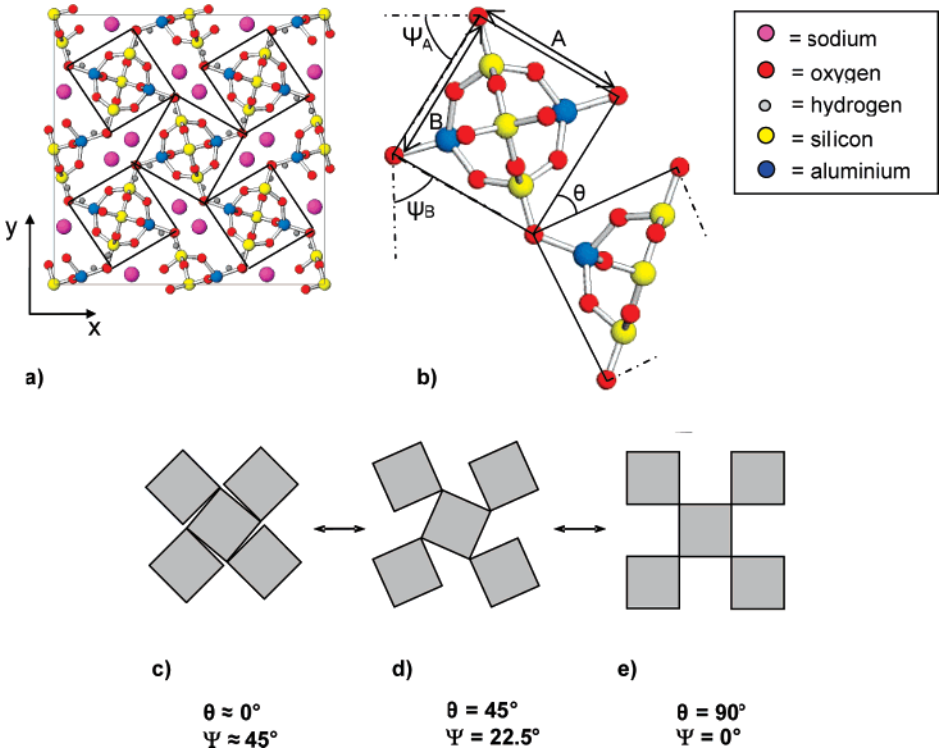

Figure 1. Illustrations of the NAT-type material natrolite containing charge-balancing sodium cations and water molecules. (a) A ball and stick representation viewed along *z* with the square cross section of columns running parallel to *z* indicated, (b) a representation of a single square column in a cross section with the Pauling angles, Ψ_a and Ψ_b, and hinge angle between the square units, θ, shown, and (c) an idealized representation of the structure showing how negative Poisson's ratio might result in the *xy* plane by application of stress.

the counterintuitive property of negative Poisson's ratio (known as auxetic materials) have been widely discussed in the literature recently because of their potential technological applications,[10−13] but generally the materials known to possess such behavior are polymers and foams where structural deformation arises on the macroscopic scale and the geometric structure needed to produce this effect is fabricated postsynthesis.[14] Simulations of the possible presence of auxetic behavior in idealized siliceous zeolites suggest that the materials might have future applications as smart filters on a molecular (or nano) scale, where molecular discriminating characteristics are adjusted by application of stress.[6]

Natrolite, $Na_2[Al_2Si_3O_{10}]\cdot 2H_2O$, is the only zeolite for which experimental elastic data have been measured from a variety of techniques, including full sets of elastic constants determined using ultrasound[15] and Brillouin scattering methods[16] and Young's moduli measured directly using micromechanical measurements.[17] The material has also been studied by crystallography under hydrostatic pressure, and although this can result in the pressure transmitting fluid being incorporated into the pores with the formation of new superhydrated phases and an unexpected volume expansion,[18−21] experimental data are available on bulk moduli at pressures below which the phase changes occur.[20] Natrolite is one of a series of a family of related minerals and synthetic materials whose general chemical composition may be written as $M_{2-2x}D_x[Al_2Si_3O_{10}]\cdot nH_2O$ (with M a monovalent ion such as Na^+, K^+, or NH_4^+ and D a divalent cation such as Ca^{2+}).[22] The common structure of these materials, with respect to the connectivity of the corner-shared tetrahedral silicate and aluminate primary building units, has been designated the NAT-type structure.[23] The NAT-type materials are examples of fibrous zeolites whose structures consist of one-dimensional chain motifs of approximate square cross section that are cross-linked to give an open net in which charge-balancing cations and, in some cases, water molecules reside, as illustrated in Figure 1. A particular interest in the elastic properties of this family of materials is the possible presence of negative Poisson's ratios in the *xy* plane (ν_{xy} and ν_{yx}).[6] This behavior has been predicted to result from the concerted rotation of the square units with

(10) Alderson, A. *Chem. Ind.* **1999**, 384.
(11) Baughman, R. H. *Nature* **2003**, *425*, 667.
(12) Stavroulakis, G. E. *Phys. Status Solidi B* **2005**, *242*, 710.
(13) Yang, W.; Li, Z.-M.; Shi, W.; Xie, B.-H.; Yang, M.-B. *J. Mater. Sci.* **2004**, *39*, 3269.
(14) Lakes, R. S. *Science* **1987**, 235, 1038.
(15) Ryzhova, T. V.; Aleksandrov, K. S.; Korobkova, V. M. *Izv. Earth Phys.* **1966**, *2*, 63.
(16) Sanchez-Valle, C.; Sinogeikin, S. V.; Lethbridge, Z. A. D.; Walton, R. I.; Smith, C. W.; Evans, K. E.; Bass, J. D. *J. Appl. Phys.* **2005**, *98*, 053508.
(17) Lethbridge, Z. A. D.; Williams, J. J.; Walton, R. I.; Smith, C. W.; Hooper, R. M.; Evans, K. E. *Acta Mater.* **2006**, *54*, 2533.
(18) Belitsky, I. A.; Fursenko, B. A.; Gabuda, S. P.; Kholdeev, O. V.; Seryotkin, Y. V. *Phys. Chem. Miner.* **1992**, *18*, 497.
(19) Colligan, M.; Lee, Y.; Vogt, T.; Celestian, A. J.; Parise, J. B.; Marshall, W. G.; Hriljac, J. A. *J. Phys. Chem. B* **2005**, *109*, 18223.
(20) Lee, Y.; Vogt, T.; Hriljac, J. A.; Parise, J. B.; Artioli, G. *J. Am. Chem. Soc.* **2002**, *124*, 5466.
(21) Seryotkin, Y. V.; Bakakin, V. V.; Fursenko, B. A.; Belitsky, I. A.; Joswig, W.; Radaelli, P. G. *Eur. J. Mineral.* **2005**, *17*, 305.
(22) Passaglia, E.; Sheppard, R. A. Zeolite Crystal Chemistry. In *Natural Zeolites: Occurence, Properties, Applications*; Bish, D. L., Ming, D. W., Eds.; Mineralogical Society of America: Washington D.C., 2001; Vol. 45, p 69.
(23) Baerlocher, C.; Meier, W. H.; Olson, D. H. *Atlas of Zeolite Framework Types*, 5th ed.; Elsevier: Amsterdam, 2001.

Table 1. Materials with the NAT-Type Structure Studied in the Present Work with Simulated and Experimental Crystal Data

material	chemical composition[a] (space group)	crystal structure reference	simulated unit cell (Å) (this work)	experimental unit cell (Å)	simulated density (g cm^{-3})	crystallographic density (g cm^{-3})
natrolite	$Na_2[Al_2Si_3O_{10}]\cdot 2H_2O$ (*Fdd2*)	27	$a = 17.920$ $b = 18.006$ $c = 6.611$	$a = 18.300$ $b = 18.630$ $c = 6.600$	2.368	2.245
mesolite	$Na_{0.67}Ca_{0.67}[Al_2Si_3O_{10}]\cdot 2.67H_2O$ (*Fdd2*)	28	$a = 18.294$ $b = 56.39$ $c = 6.615$	$a = 18.405$ $b = 56.655$ $c = 6.5443$	2.268	2.268
scolecite	$Ca[Al_2Si_3O_{10}]\cdot 3H_2O$ (*F1d1*)	29	$a = 18.449$ $b = 19.01$ $c = 6.622$	$a = 18.502$ $b = 18.974$ $c = 6.525$	2.275	2.244
metanatrolite	$Na_2[Al_2Si_3O_{10}]$ (*F112*)	26	$a = 16.345$ $b = 16.746$ $c = 6.547$	$a = 16.244$ $b = 17.018$ $c = 6.430$	2.244	2.54
ammonium natrolite	$(NH_4)_2[Al_2Si_3O_{10}]$ (*C1121*)	30	$a = 17.662$ $b = 18.216$ $c = 6.616$	$a = 17.899$ $b = 18.390$ $c = 6.529$	2.090	2.066

[a] Chemical compositions are written to express relative number of extraframework species per aluminosilicate unit $[Al_2Si_3O_{10}]^{2-}$ of the framework.

respect to each other upon application of stress, as indicated in Figure 1.[24] In fact, the initial angle between the square units varies in the NAT family depending upon the cation content and the amount of crystal water. This was first proposed by Pauling in the 1930s,[25] and the extent of rotation of the square cross-section columns may be defined using the "Pauling chain rotation angle". Thus, a structural deformation corresponding to rotation of the square units can be chemically induced by ion exchange.

Given the range of extraframework species that can be incorporated into the NAT framework, the availability of full crystallographic data for several members of the family, and experimental elastic constants for natrolite itself, this group of materials provides an opportunity for a systematic study of the effect of extraframework species upon the elasticity of a aluminosilicate framework. We have recently successfully used the Cerius[2] package, which allowed implementation of the CVFF 300 force field, to simulate the elastic properties of natrolite itself and a hypothetical siliceous form of the NAT-type structure, which has no charge-balancing cations, to back up our experimental studies of mechanical and elastic properties.[17] We now extend the modeling approach to consider four other members of the NAT family and include new simulations of the off-axis elastic properties of all the materials. The materials we will describe in this paper are listed in Table 1; each has been studied using crystallography previously by a number of groups and each has precisely defined concentrations of extraframework cations whose location (including hydrogen atoms of water molecules) has been accurately determined. The material metanatrolite is a dehydrated form of natrolite, but is stable under ambient temperature and pressure if water is excluded.[26] The aim of our work was to predict and understand possible atomic-scale structural deformation mechanisms of the NAT materials, in particular, to examine the preliminary predictions of their possible auxetic properties. Our discussion will thus largely be focused on the elastic behavior of the materials to stress in the plane of the "rotating square" units.

Modeling Methodology

Simulations of Elasticity. Computer simulations were carried out using the molecular modeling package Cerius[2] v 4.8.1 (Accelrys., San Diego, CA) running on an Octane SE workstation running Irix 6.5a. The starting structures of the zeolites, taken from crystallographic data available in the literature, were input into Cerius[2] for the materials natrolite,[27] mesolite,[28] scolecite,[29] metanatrolite,[26] and ammonium-exchanged natrolite[30] (see Table 1, where their chemical compositions are also given). Charges were assigned to the water molecules (-0.82 for oxygen and $+0.41$ for hydrogen) and ammonium ions (-0.12 for nitrogen and $+0.28$ for hydrogen). Sodium ions were assigned a charge of $+1$ and calcium ions were assigned a charge of $+2$. Partial charges for the zeolite framework were assigned using the Burchart-Dreiding force field:[31] the values employed in the simulations were Si $= +0.224$, Al $= +0.394$, and O $= -0.346$. Charges were then averaged to zero over the entire framework. The energy expressions E were set up using parameters from CVFF (consistent valence-field force field).[32] This force field was originally developed for small organic molecules but has been developed for materials science applications including the simulation of aluminosilicate zeolite structures and other extended oxide networks, for which it has been successfully applied recently.[33−35] The parameters used to simulate the zeolite framework were the default ones provided by Cerius[2] for the "CVFF_300" force field; they have been optimized for zeolitic

(24) Grima, J. N.; Evans, K. E. *J. Mater. Sci. Lett.* **2000**, *15*, 475.
(25) Pauling, L. *Proc. Natl. Acad. Sci. U.S.A.* **1930**, *16*, 453.
(26) Baur, W. H.; Joswig, W. *N. J. Miner. Monat.* **1996**, 171.
(27) Torrie, B. H.; Brown, I. D.; Petch, H. E. *Can. J. Phys.* **1964**, *42*, 229.
(28) Stuckenschmidt, E.; Kirfel, A. *Eur. J. Mineral.* **2000**, *12*, 571.
(29) Stuckenschmidt, E.; Joswig, W.; Baur, W. H.; Hofmeister, W. *Phys. Chem. Miner.* **1997**, *24*, 403.
(30) Stuckenschmidt, E.; Kassner, D.; Joswig, W.; Baur, W. H. *Eur. J. Mineral.* **1992**, *4*, 1229.
(31) Burchart, E. D.; Verheij, V. A.; Vanbekkum, H.; Vandegraaf, B. *Zeolites* **1992**, *12*, 183.
(32) Hagler, A. T.; Huler, E.; Lifson, S. *J. Am. Chem. Soc.* **1974**, *96*, 5319.
(33) Kim, N.; Kim, Y.; Tsotsis, T. T.; Sahimi, M. *J. Chem. Phys.* **2005**, *122*, 214713.
(34) Moloy, E. C.; Cygan, R. T.; Bonhomme, F.; Teter, D. M.; Navrotsky, A. *Chem. Mater.* **2004**, *16*, 2121.
(35) Moloy, E. C.; Davila, L. P.; Shackelford, J. F.; Navrotsky, A. *Microporous Mesoporous Mater.* **2002**, *54*, 1.

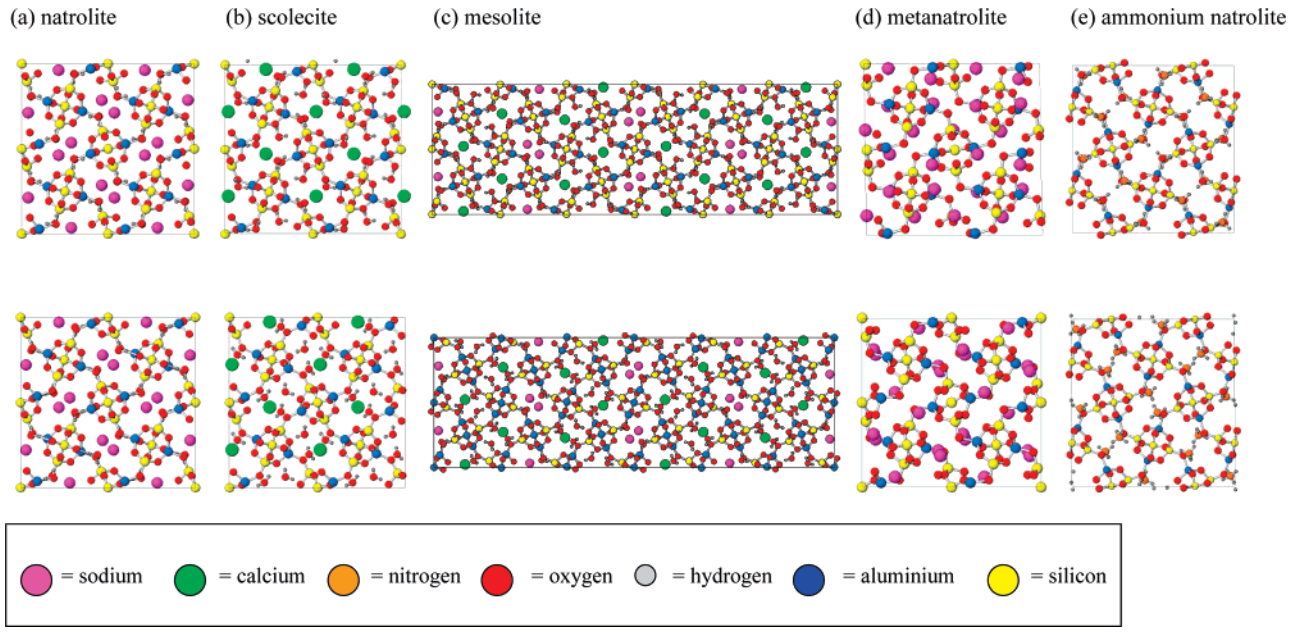

Figure 2. Comparison of representative portions (viewed in the *xy* plane, along 001) of the simulated (top) and experimental (bottom) NAT-type materials: (a) natrolite, (b) scolecite, (c) mesolite, (d) metanatrolite, and (e) ammonium natrolite.

systems and are the same ones previously used by De Luca et al. who studied the structures of the zeolite silicalite and silica-sodalite.[36] Minimum energy configurations were derived by minimizing the potential energy as a function of the atomic coordinates and unit cell parameters to the default Cerius[2] high-convergence criterion (which include an atomic root-mean-square of the derivative of the energy expression of less than 0.001 kcal mol^{-1} Å^{-1}). No constraints on the shape or size of the unit cell were applied during minimization. The 6 × 6 stiffness matrix, **C** (and its inverse, the compliance matrix, **S**), of the minimum-energy, single-crystalline system was calculated for each zeolite from the second derivative of the potential energy function since

$$c_{ij} = \frac{1}{V}\frac{\partial^2 E}{\partial\epsilon_i \partial\epsilon_j} \quad i,j = 1, 2, ..., 6 \tag{1}$$

where c_{ij} is an element of the stiffness matrix, E is the energy expression, V is the volume of the unit cell, and ϵ_i and ϵ_j are strain components.

The Poisson's ratios ν_{ij} in the Ox_i−Ox_j planes (i,j = 1,2,3) for loading in the Ox_i directions are then given by

$$\nu_{ij} = -\frac{\text{transverse strain}}{\text{axial strain}} = -\frac{\epsilon_j}{\epsilon_i} = -\frac{s_{ij}}{s_{ii}} \tag{2}$$

and the Young's moduli E_i (a measure of the stiffness) for loading in the Ox_i (I = 1,2,3) directions are given by

$$E_i = \frac{\text{applied stress}}{\text{axial strain}} = \frac{\sigma_i}{\epsilon_i} = \frac{1}{s_{ii}} \tag{3}$$

where s_{ij} is an element of the compliance matrix.

The bulk modulus can also be calculated from the compliance matrix as follows:

$$K = \frac{1}{s_{11} + s_{22} + s_{33} + 2[s_{31} + s_{21} + s_{32}]} \tag{4}$$

To allow comparison with the crystal structures, the Poisson's ratios are hereafter expressed in terms of the crystal coordinate system (x,y,z) such that $\nu_{12} = \nu_{xy}$ etc. and the Young's moduli E_i are expressed as E_x, E_y, and E_z.

Application of stress in three perpendicular directions was simulated using the molecular dynamics method of Parrinello and Rahman,[37,38] which allows both the size and shape of the cell to change so that the internal stress of the system can match the externally applied stress. Here, an additional energy term due to the externally applied stress is added and the effect on the shape and size of the unit cell is obtained from running the molecular dynamic simulation to equilibrium. The edges of the unit cell a, b, and c are treated as dynamical variables. These variables are arranged to form a 3 × 3 matrix h and the work of Anderson,[39] which allows volume but not shape changes of the unit cell, is extended to include changes in the volume and shape of the unit cell. The Parrinello and Rahman method introduces a Langrangian that couples the h degrees of freedom with the microscopic motion of the atoms under the condition of constant pressure. The size and shape of the unit cell can change so that the internal stress of the system can match the externally applied stress, according to the dynamical equations given by the Langrangian. As well as allowing a visual representation of possible atomic-level distortions, this approach provides an independent means of calculating elastic constants since the change of size of unit cell parameters with application of known stress provides a strain ratio which allows Poisson's ratios and Young's moduli to be determined.

Off-Axis Elastic Behavior. The effect of rotating the direction of applied stress with respect to the crystallographic axes was also investigated. The standard set of transformation equations[40,41] were used to rotate the elements of the computed or measured stiffness (or compliance) matrix through a specified angle about a defined axis. The elastic properties of the system could then be calculated for a specific angle of rotation or plotted for a range of angles about an axis.

(36) De Luca, G.; Pullumbi, P.; Barbieri, G.; Fama, A. D.; Bernardo, P.; Drioli, E. *Sep. Purif. Technol.* **2004**, *36*, 215.
(37) Parrinello, M.; Rahman, A. *J. Appl. Phys.* **1981**, *52*, 7182.
(38) Parrinello, M.; Rahman, A. *Phys. Rev. Lett.* **1980**, *45*, 1196.
(39) Andersen, H. C. *J. Chem. Phys.* **1980**, *72*, 2384.
(40) Hearmon, R. F. S. *Rev. Mod. Phys.* **1946**, *18*, 409.
(41) Hearmon, R. F. S. *Adv. Phys.* **1956**, *5*, 323.

Table 2. Simulated and Experimental Pauling Angles and Parameters Describing Chain Cross Section (see Figure 1 for Definitions)

material	experimental "square" dimensions (Å²)	simulated "square" dimensions (Å²)	experimental Ψ_a (deg)	simulated Ψ_a (deg)	experimental Ψ_b (deg)	simulated Ψ_b (deg)	experimental average Ψ (deg)	simulated average Ψ (deg)
natrolite	5.0455 × 5.0696	5.1177 × 5.0588	24.940	28.910	23.260	27.145	24.100	28.028
mesolite	4.9822 × 4.9710	5.0592 × 5.0849	21.138	23.021	20.010	23.021	20.617	23.021
scolecite	4.9938 × 4.9767	5.0518 × 5.1211	20.676	23.918	20.046	22.093	20.361	23.005
metanatrolite	4.9304 × 5.0411	5.1741 × 5.1178	34.813	37.239	32.294	35.338	33.553	36.288
ammonium natrolite	5.0537 × 5.0427	5.0723 × 5.1437	26.258	29.709	25.008	27.687	25.633	28.698

Table 3. Some Predicted Elastic Properties of the NAT Zeolites (Experimental Values for Natrolite from Brillouin Scattering[16] Are Given in Parentheses)

	C_{ij} (GPa)									bulk modulus (GPa)
material	C_{11}	C_{22}	C_{33}	C_{44}	C_{55}	C_{66}	C_{12}	C_{13}	C_{23}	
natrolite	89.4	84.7	200.6	30.7	32.6	61.3	21.7	38.5	36.5	52.8
	(70.4)	(72.0)	(132.3)	(26.8)	(26.5)	(51.3)	(26.0)	(32.8)	(31.8)	(48.5)
mesolite	80.0	75.0	186.5	25.9	26.9	61.0	29.9	32.7	37.1	51.4
scolecite	75.2	83.6	183.0	26.8	27.6	61.6	32.9	29.7	39.4	49.5
metanatrolite	33.1	36.4	209.3	18.7	20.3	57.7	11.0	22.8	17.0	21.8
ammonium natrolite	38.4	44.9	192.2	13.7	32.1	58.3	6.5	15.4	16.4	23.6

Table 4. Simulated On-Axis Poisson's Ratios and Young's Moduli of the NAT Zeolites; Experimental Data Are Also Given for Natrolite

material	method	ν_{xy}	ν_{yx}	ν_{zx}	ν_{xz}	ν_{yz}	ν_{zy}	E_x (GPa)	E_y (GPa)	E_z (GPa)
natrolite	experimental data	0.28	0.29	0.18	0.36	0.17	0.31	57.14	59.17	111.1
	strain independent; second derivative method	0.189	0.180	0.347	0.157	0.148	0.342	79.262	75.436	174.775
	change in cell parameters, 0.1 GPa stress	0.188	0.178	0.351	0.156	0.146	0.340	78.910	75.049	175.030
	change in cell parameters, 1 GPa stress	0.171	0.167	0.346	0.143	0.133	0.341	74.303	70.757	176.028
mesolite	strain independent; second derivative method	0.345	0.319	0.267	0.107	0.143	0.389	65.181	60.203	163.302
	change in cell parameters, 0.1 GPa stress	0.344	0.319	0.267	0.106	0.142	0.387	64.828	59.999	163.140
	change in cell parameters, 1 GPa stress	0.330	0.312	0.266	0.097	0.136	0.386	61.313	58.080	164.511
scolecite	strain independent; second derivative method	0.334	0.347	0.223	0.084	0.146	0.373	60.574	62.878	161.026
	change in cell parameters, 0.1 GPa stress	0.332	0.348	0.224	0.084	0.146	0.361	60.374	62.683	161.197
	change in cell parameters, 1 GPa stress	0.312	0.355	0.222	0.078	0.139	0.372	56.524	60.242	162.081
metanatrolite	strain independent; second derivative method	0.511	0.441	0.487	0.058	0.048	0.463	22.421	19.350	187.018
	change in cell parameters, 0.1 GPa stress	0.577	0.392	0.473	0.055	0.050	0.478	19.760	18.643	187.101
	change in cell parameters, 1 GPa stress	0.135	0.276	0.494	0.073	0.079	0.468	17.233	24.077	187.858
ammonium natrolite	strain independent; second derivative method	0.118	0.138	0.349	0.070	0.074	0.315	36.598	42.802	181.687
	change in cell parameters, 0.1 GPa stress	0.101	0.123	0.351	0.070	0.074	0.308	36.070	42.381	181.966
	change in cell parameters, 1 GPa stress	−0.567	−1.037	0.345	0.101	0.119	0.311	9.488	11.622	182.634

Results and Discussion

1. Simulations of Atomic Structure and Elastic Constants. The simulated unit cell parameters and densities of the crystal structures of the five NAT materials we have studied are compared with experimental parameters in Table 1. For all of the structures, the simulated cell parameters agree within 3% of the experimental parameters, typical agreement for force-field simulations. Figure 2 shows a comparison of representative portions of the structures, illustrating qualitatively the good agreement between experimental and simulated structural models. Simulated and experimental atomic coordinates are available as Supporting Information, where the excellent quantitative agreement between them is shown. Bond angles and bond lengths for the experimental and simulated structures are also compared in the Supporting Information. All bond distances within the framework agree within 0.1 Å of the experimental values determined by crystallography and all bond angles agree within 4°. There is slightly larger discrepancy in the bond distances involving extraframework species, compared to

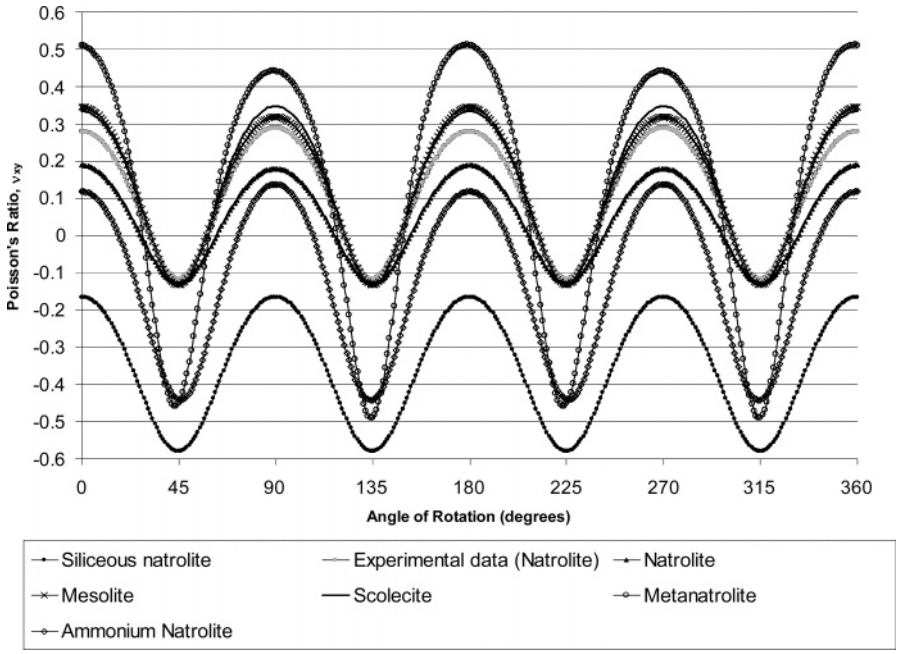

Figure 3. Cartesian representation of simulated off-axis plots of ν_{xy} upon rotation about the *z*-axis for the NAT series.

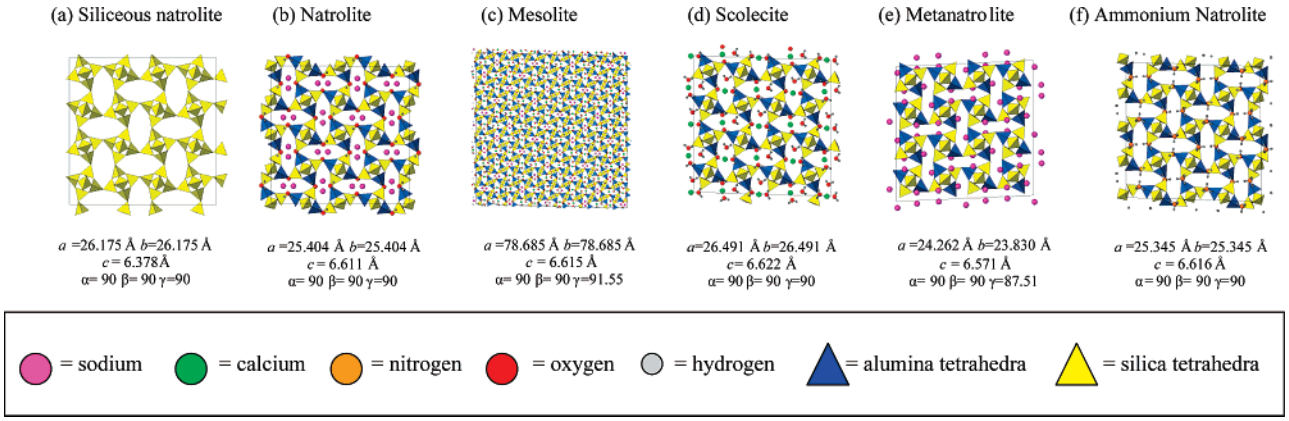

Figure 4. "Rotated" unit cells for the NAT-type materials for analysis of off-axis elastic properties.

those involving framework atoms, and this may reflect the increased mobility of ions and water molecules within the zeolite pores over those atoms which form part of the framework. It is noteworthy, however, that the force-field approach predicts successfully the relative location of the extraframework species.

As was mentioned in the Introduction, an additional parameter that can be used to describe the NAT-type structure is the "Pauling chain rotation angle", Ψ, which defines the relative orientation of the square cross-section chain in the *xy* plane to the unit cell edges *a* and *b*, as shown in Figure 1. In fact, the unit cells of the NAT-type materials are orthorhombic and not tetragonal, and so the "square" units are actually quadrilaterals (with the edge lengths close to equal and the internal angles close to 90°); this results in two angles, Ψ_a and Ψ_b, defining the relative orientation of the quadrilateral edges to the *a* and *b* unit cell edges, respectively, and it is the average of these that is usually quoted. Using the atomic coordinates of the projection of the NAT-type columns (i.e., the *x* and *y* coordinates of the oxygen atoms defining the corners of the 'squares'), we have thus calculated values of Pauling chain rotation angles for each of the NAT materials and compared simulation with the crystallographic data; these values are shown in Table 2, along with the edge lengths of the "square" cross section. Although the simulated values of average Pauling angle show some small discrepancy with the experimental values, all being up to 4° larger than those found by crystallography, importantly, the predicted values follow the general order for the series of materials, with scolecite having the smallest Pauling angle and metanatrolite the largest.

Elastic constants determined from the second derivative of the minimized energy are tabulated in Table 3, along with the bulk modulus for all of the materials studied. Only for natrolite have experimental values of these parameters been determined, and we have recently published a comparison of the simulated and experimental values for this particular material:[17] this is reproduced in Table 3. The experimental values of elastic constants (elements of the stiffness matrix, C_{ij}, and its inverse, the compliance matrix) were measured by determining acoustic velocities from a natural, single-crystal specimen of natrolite.[16] Inversion of the acoustic velocity data allowed the determination of the full set of nine unique elastic constants for orthorhombic natrolite, and then with use of standard relationships, values of elastic moduli could be calculated.[16] For further comparison, the

Table 5. Off-Axis (45°) Poisson's Ratios and Young's Moduli of NAT-Type Zeolites Calculated Using the Minimized Energy of the Rotated Units Cell, from Changes in the Cell Parameters on Application of Stress, and from Standard Transformation on the Predicted and Measured Elastic Constants

material	method	ν_{xy}	ν_{yx}	ν_{zx}	ν_{xz}	ν_{yz}	ν_{zy}	E_x (GPa)	E_y (GPa)	E_z (GPa)
natrolite	transformation of experimental values[16]	−0.115	−0.115	0.332	0.272	0.272	0.332	90.781	90.781	110.807
	transformation of modeled elastic constants	−0.128	−0.128	0.344	0.211	0.211	0.344	106.877	106.877	174.776
	strain independent; second derivative method	−0.128	−0.128	0.344	0.211	0.211	0.344	106.890	106.851	174.779
	change in cell parameters, 0.1 GPa stress	−0.130	−0.130	0.344	0.210	0.210	0.344	106.704	106.600	174.984
	change in cell parameters, 1 GPa stress	−0.149	−0.147	0.343	0.205	0.203	0.343	105.037	104.018	175.972
mesolite[a]	strain independent; second derivative method	–	–	–	–	–	–	–	–	–
	change in cell parameters, 0.1 GPa stress	−0.133	−0.135	0.320	0.212	0.213	0.320	105.811	105.542	163.382
	change in cell parameters, 1 GPa stress	−0.144	−0.145	0.328	0.209	0.209	0.328	105.400	104.107	164.556
	transformation of modeled elastic constants	−0.132	−0.132	0.328	0.213	0.213	0.328	105.975	105.975	163.303
scolectite	strain independent; second derivative method	−0.134	−0.134	0.296	0.195	0.198	0.300	105.949	106.153	161.020
	change in cell parameters, 0.1 GPa stress	−0.134	−0.135	0.300	0.195	0.197	0.300	106.389	106.110	161.118
	change in cell parameters, 1 GPa stress	−0.144	−0.142	0.299	0.194	0.195	0.299	105.930	104.954	162.108
	transformation of modeled elastic constants	−0.135	−0.135	0.298	0.196	0.196	0.298	106.117	106.117	161.025
metanatrolite	strain independent; second derivative method	−0.445	−0.411	0.250	0.139	0.149	0.408	77.713	71.648	196.013
	change in cell parameters, 0.1 GPa stress	−0.436	−0.444	0.351	0.137	0.151	0.407	76.339	72.407	196.447
	change in cell parameters, 1 GPa stress	−0.419	−0.433	0.352	0.137	0.161	0.409	77.285	77.229	196.936
	transformation of modeled elastic constants	−0.451	−0.490	0.465	0.139	0.157	0.485	55.707	60.471	187.017
ammonium natrolite	strain independent; second derivative method	−0.439	−0.442	0.333	0.119	0.119	0.331	64.804	65.359	181.685
	change in cell parameters, 0.1 GPa stress	−0.453	−0.451	0.333	0.118	0.118	0.333	63.811	63.900	183.684
	change in cell parameters, 1 GPa stress	−0.988	−0.904	0.328	0.124	0.114	0.328	11.815	10.816	182.639
	transformation of modeled elastic constants	−0.441	−0.441	0.119	0.332	0.119	0.332	65.162	65.161	181.686

[a] For the large "rotated" unit cell of mesolite, the calculation did not reach completion.

experimental value for the bulk modulus determined during high pressure (hydrostatic) powder X-ray diffraction studies of natrolite is 53(1) GPa,[20] with which the simulated value shows very good agreement. The good agreement between the experimental and simulated values of elastic data for natrolite gives us further confidence in interpreting the simulation results for the other members of the NAT family.

Table 4 contains the on-axis Poisson's ratios calculated from the simulated stiffness matrices (also compared to values determined using the change in cell parameters upon simulated application of stress as described below). Thus, the elastic constants in Table 3 imply that the Poisson's ratios of all members of the NAT family are positive "on-axis" (that is, when stress is applied parallel to any of the three crystallographic axes).

We note here that the predicted elastic constants, bulk moduli (Table 3), Young's moduli, and Poisson's ratios (Table 4) for the materials mesolite and scolecite are rather similar to the values for natrolite itself, despite the fact that different extraframework species are present. Whereas natrolite contains Na^+ cations balancing the negative charge of the aluminosilicate framework, scolecite contains Ca^{2+} ions, and mesolite represents the intermediate situation, containing both Ca^{2+} and Na^+.[28] Although half as many divalent Ca^{2+} ions as monovalent Na^+ ions are necessary to balance the charge of the aluminosilicate framework, the three materials contain different amounts of water: it can be seen by their chemical formulas that, for each pair of Na^+ ions replaced by a Ca^{2+}, an additional extraframework water molecule is also occluded. Thus, the extraframework void space is filled by a total number of species that occupy a similar volume: the NAT framework is little disrupted by the ion-exchange process and all three materials have similar Pauling angles defining the "openness" of the network of linked squares. Despite the fact that Ca^{2+} has a larger charge density than Na^+ (their ionic radii being similar), the similar values for bulk and Young's moduli of the series natrolite−mesolite−scolecite would suggest that it is the total volume of extraframework species that affects the elastic constants of the NAT-type materials, rather than their charge or charge density.

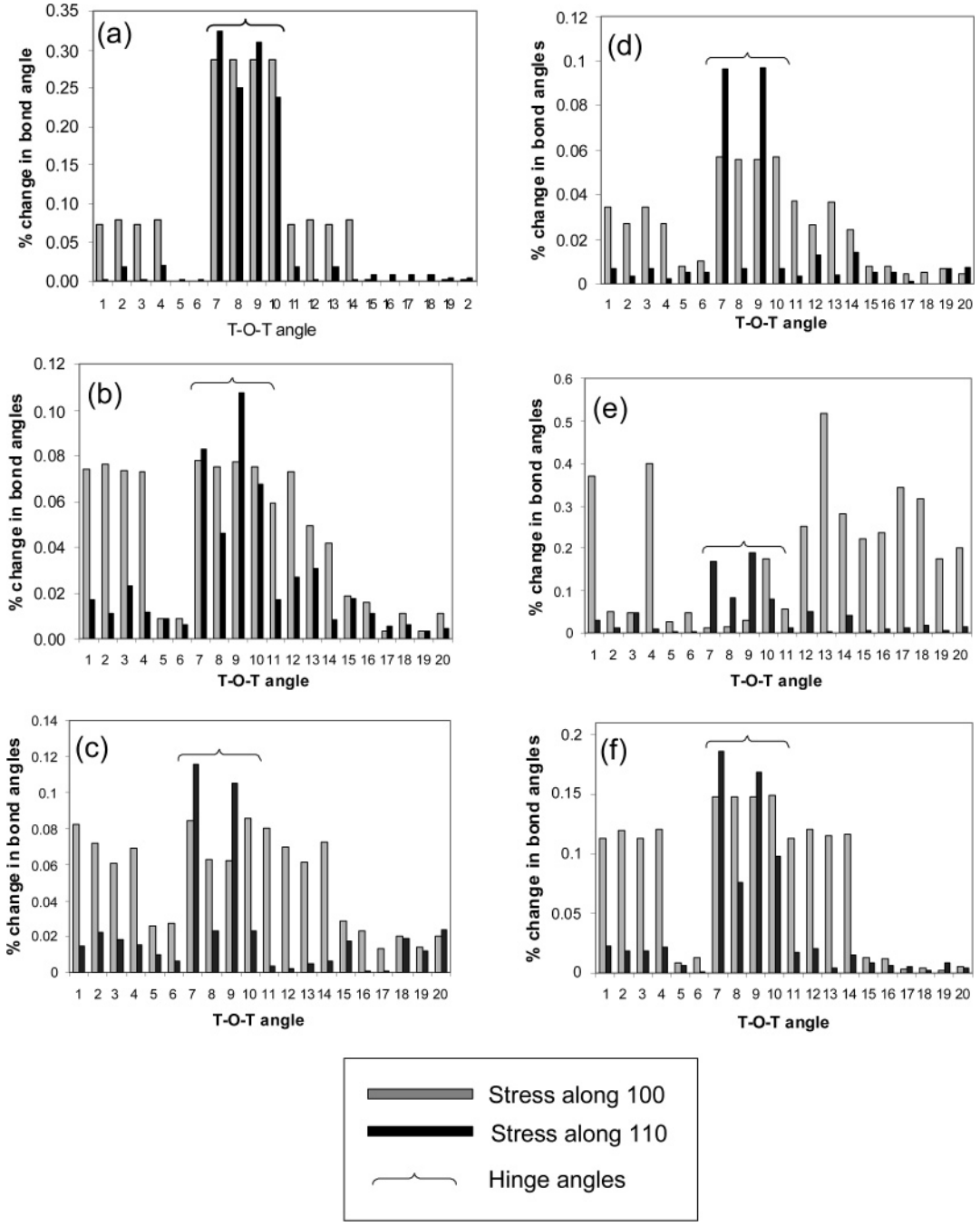

Figure 5. Bar charts of percentage change in bond angles in the NAT-type materials on simulated application of stress along *x* and at 45° to *x* for (a) siliceous natrolite, (b) natrolite, (c) mesolite, (d) scolecite, (e) metanatrolite, and (f) ammonium natrolite. Hinge angles are indicated.

Examining the data for the materials metanatrolite and ammonium natrolite, which contain fewer extraframework species, backs up this view: the former is a dehydrated form of natrolite and contains just Na^+ without extraframework water, while the latter contains just NH_4^+. This pair of materials has noticeably lower bulk moduli and Young's moduli than the materials natrolite, mesolite, and scolecite. This could be attributed to two (related) factors: either the larger Pauling angles of these two materials compared to natrolite, mesolite, and scolecite, reflecting a closing up of the network of square units, or the presence of fewer extraframework species, which might allow a more free rotation of the tetrahedral framework upon application of stress.

We now consider off-axis Poisson's ratios. When standard transformation matrices are applied to the simulated elastic constants, it is found that for the series of NAT-type zeolites the Poisson's ratios ν_{xy} and ν_{yx} become negative when rotated off-axis about the *z*-axis. The Poisson's ratios reach their most negative value at 45° for each of the NAT zeolites, that is, maximum auxetic behavior would be observed in the *xy* plane for stretching (or compressing) at 45° to either the *x* or *y* axes. This is illustrated as a series of Cartesian plots in Figure 3 for the Poisson's ratio ν_{xy}, which also includes a plot derived from the experimental elastic constants for natrolite. This allows a direct comparison of the same off-axis behavior of each of the NAT-type zeolites and clearly shows how, for all the zeolites, the general trend

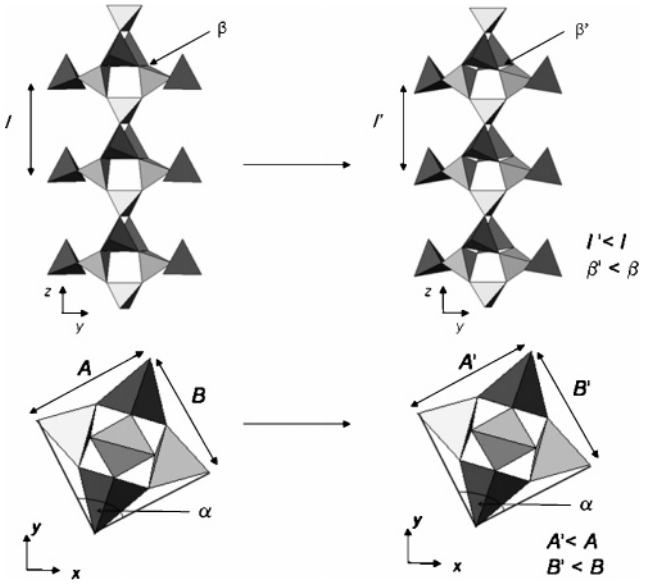

Figure 6. View of a single chain of NAT, indicating how distortions within the NAT chain (changes in l and β) can adjust the dimensions of the chain cross section (A, B, and α).

of a maximum negative Poisson's ratio at 45° and a maximum positive value on-axis at 0° is found. While natrolite, mesolite, and scolecite have rather similar Poissons' ratios which all vary in a similar magnitude upon the change of angle of applied stress, the materials metanatrolite and ammonium natrolite show rather different behaviors, with a more pronounced negative Poisson's ratio. This is in line with the observation made above regarding Bulk and Young's moduli. For comparison, the simulated off-axis values for the Poisson's ratio ν_{xy} for a hypothetical siliceous form of natrolite are also presented in Figure 3. In this case, although the Poisson's ratio is predicted to always be negative, the off-axis graph shows exactly the same trend as for the other NAT materials with the most negative Poisson's ratio seen when stress is applied at 45° to the x-axis (in the case of ν_{xy}). It is worth recalling at this point that the idealized "rotating squares" model for negative Poisson's ratio behavior previously elaborated by Grima and co-workers,[24] and depicted in Figure 1, predicts a value of $\nu_{xy} = \nu_{xy} = -1$ at all orientations of applied stress. Our considerations suggest that the presence of extraframework cations and water molecules is a highly important factor in determining the absolute values of Poisson's ratios, and also that the frameworks of the NAT-type materials respond in a more complex manner upon application of applied stress, not just involving the rotation of square units about their hinges, whether or not extraframework species are present.

2. Simulations of Atomic-Scale Elastic Deformation. To better understand the predicted elastic constants and their off-axis behavior, the response of the NAT-type materials to uniaxial stress in various directions was also simulated, by using the molecular dynamics method of Parrinello and Rahman.[37] The cell parameters of the NAT-type structures with applied stress in the x, y, and z directions are presented as Supporting Information. The Poisson's ratio can also be calculated from the change in the cell parameters on the application of stress and this serves as an independent means of determining these parameters to compare with those calculated from the second derivative of the minimized energy of the atomic simulation, and the Poisson's ratios calculated using each of these methods are compared in Table 5. Excellent agreement is observed in the Poisson's ratios calculated using the different methods, and in the case of natrolite, for which experimental values of the elastic constants have been published, good agreement with the experimentally derived Poisson's ratios is also achieved. These considerations give us confidence that the Parrinello and Rahman method is accurately predicting atomic-scale deformations upon application of stress and that we can use the atomic movement predicted on application of stress to produce structural models to explain the elastic behavior of the materials.

It should be noted that, on addition of stresses larger than 0.1 GPa to ammonium-exchanged natrolite and metanatrolite, with use of the method of Parrinello and Rahman, the frameworks are seen to open out significantly more than natrolite, mesolite, or scolecite: there are large increases in the cell parameters (Supporting Information) and the densities of the materials decrease. As was noted above, ammonium-exchanged natrolite and metanatrolite contain fewer extra-framework species, and it can be envisaged that on application of a large stress, the effects of extraframework cations and water are reduced and the structures become freely rotating. The increased structural flexibility of ammonium natrolite and metanatrolite is reflected in their low Young's moduli (Table 4) and low bulk moduli (Table 3) and is also reflected in the values of the Poisson's ratios calculated from the cell parameters when a 1GPa stress is applied. The on-axis values of ν_{xy}, ν_{yx} approach those values calculated for an off-axis stress at 45° (Table 5), suggesting a rotational effect is dominant in these structures both on- and off-axis when larger stresses are applied. In the case of ammonium natrolite in particular, the values of ν_{xy}, ν_{yx} calculated for a 1 GPa stress approach -1, indicating that this framework is behaving much like an idealized rotating squares model.

To further investigate the maximum auxetic behavior that is predicted off-axis, the response of the structures to a stress applied at 45° was examined. Here the unit cell of each material was redefined such that the original contents were rotated 45° with respect to their original axes, resulting in a new, larger unit cell. These "rotated" unit cells are illustrated in Figure 4. Applying a stress parallel to either x or y in each of these redefined unit cells is equivalent to applying a stress at 45° to the axes of the original unit cell. The cell parameters of each of these NAT-type zeolites as stress is applied are presented as Supporting Information, and Table 5 contains the Poisson's ratios determined by the change in cell parameters compared to those produced from the second derivative of the minimized energy of the redefined unit cell. For a final comparison, the off-axis Poisson's ratios produced by application of standard transformation matrices to the values determined for the zeolite structures in Table 4 are also shown in Table 5: this demonstrates the self-consistency of the approach.

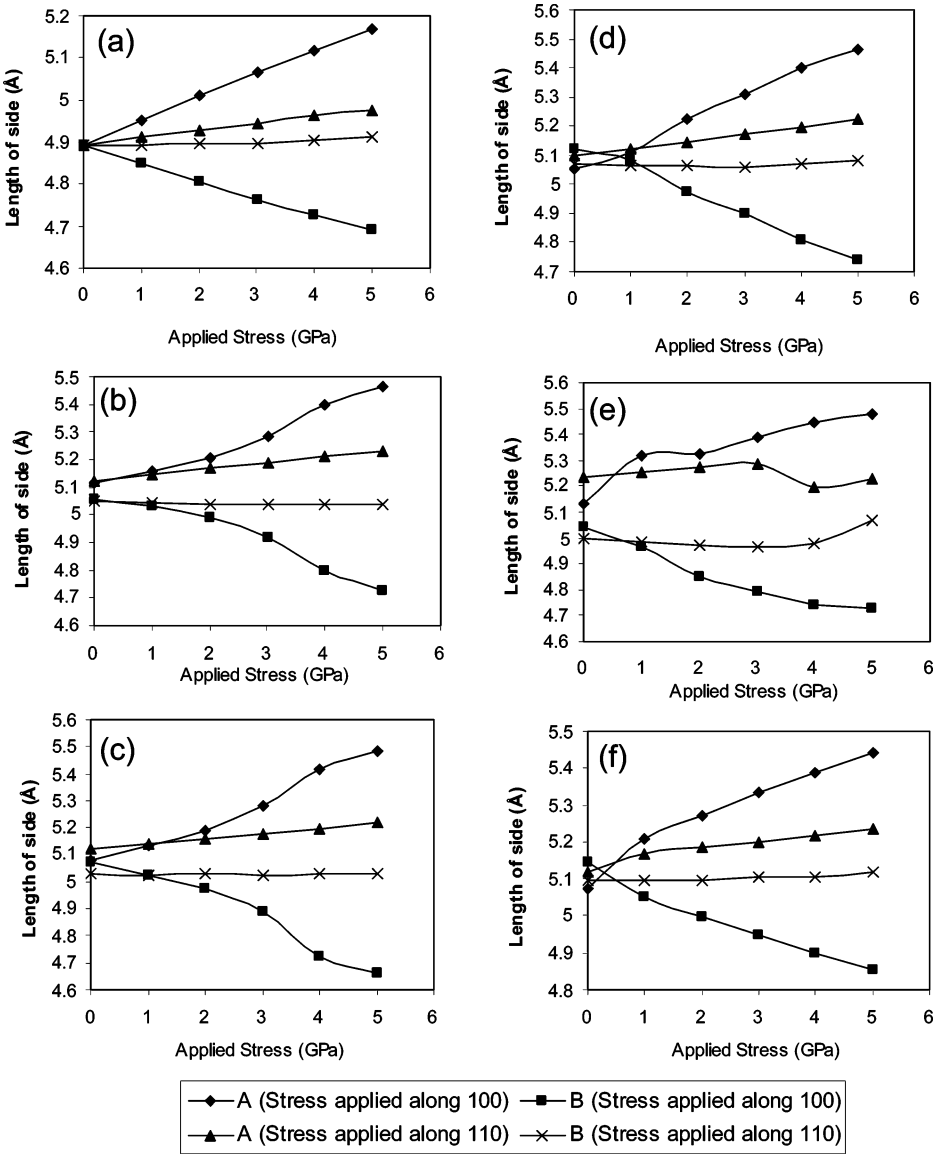

Figure 7. Change in the edge lengths of chain cross section for the NAT zeolites: (a) siliceous natrolite, (b) natrolite, (c) mesolite, (d) scolecite, (e) metanatrolite, and (f) ammonium natrolite upon simulated application of stress in *x* and at 45° to *x*.

The bond angles and bond lengths for the five zeolite structures when a 1 GPa stress is applied in the *x*, *y*, and *z* directions are presented in Supporting Information, compared to those of the initial, minimized structure. Bond distances and bond angles fall within reasonable limits and do not vary significantly from those of the simulated structure. Bond angles and bond lengths of the stressed structures are typically within 0.5% of those of the simulated structure. The fact that both Si−O and Al−O bonds and intratetrahedral O−Si−O and O−Al−O angles remain approximately fixed indicates that, to a first approximation, we can deal with models that consider rigid tetrahedral units. Similarly, upon application of stress at 45° to the principal crystallographic axes, the interatomic distances and angles defining the tetrahedral building units also remain approximately fixed (see Supporting Information). It is therefore clear that the bond angles defining the linkages between the $\{SiO_4\}$ and $\{AlO_4\}$ tetrahedral units are important to consider if an atomic-scale model for structural deformation with stress is to be proposed: that is, a rigid-unit model. For natrolite, scolecite, metanatrolite, and ammonium-natrolite, there are 20 unique inter-tetrahedral angles defining the three-dimensional network structure. For mesolite, the situation is more complex since the extraframework void space contains alternating sodium and calcium ions in neighboring channels, Figure 2c; thus, tetrahedral units in each chain of the structure do not all have the same environment. A single, representative chain unit was therefore selected here for the measurement of changing bond angles with stress: this was one surrounded by two sodium ions and a single calcium. The percentage changes in these inter-tetrahedral angles as stress of 0.1 GPa is applied on-axis, and at 45° off-axis, are represented in Figure 5 as a bar chart for each of the NAT materials, with the angles that correspond to the "hinge" between the square units highlighted (the remaining angles correspond to those within the square cross sections or along the chain axis). This shows that, for all of the NAT-type zeolites considered, the hinge angles are those that exhibit the largest percentage changes upon application of stress at 45° to the *x*-axis (in the (110) or (1−10) directions), whereas

upon application of stress along the *x*-axis (on-axis) the hinge angles change with amounts comparable to, or much less than, the other angles defining the structure. This is consistent with our observation that negative Poisson's ratios ν_{yx} are found at 45°: here, the hinge angle appears to dominate structural change, resulting in the rotation of the squares, rather than some other distortion of the structure. For the hypothetical siliceous form of NAT, which contains no extraframework species, the hinge angles always change by the largest percentage whether the stress is applied on-axis or at 45° to the axes: this is consistent with the fact that Poisson's ratios are expected to always be negative for this material.

It is also important to note that while the hinge angle between the rotating square units changes upon application of stress along *x* or at 45° to *x*, all other inter-tetrahedral angles also change. As indicated by Figure 6, the effect of deformations along the chain (which runs parallel to *z*), even when stress is applied along *x* or *y*, is to distort the square cross section. To simplify the discussion of this effect, we have therefore reduced the three-dimensional effect to a two-dimensional model in the *xy*-plane and thus consider the dimensions of the "square" cross section and how this changes upon application of stress. The changing "square" dimensions with applied stress are shown graphically in Figure 7 which demonstrates how the lengths of the sides of the square cross section change upon application of increasing stress. (Note that the maximum stress applied of 5 GPa is less than the hydrostatic pressure of 6−7 GPa that causes amorphization of natrolite.[42]) For each of the zeolites, an off-axis stretch at 45° causes much less distortion of the square units (i.e., changes of the length of edges) than an on-axis stretch in *x*. This is actually predicted whether or not extraframework species are present, as shown by the simulations of the behavior of the hypothetical siliceous NAT structure, which has a neutral framework and hence no charge-balancing species nor any extraframework water molecules. A similar effect can be observed when a rotation-dominated, physical model (such as a cardboard model) of a rotating squares network is pulled: there is much less resistance when the model is pulled open along the diagonal rather than along the horizontal (the diagonal direction being that which crosses the void space between the square units, see Figure 1a). That is, a moment is more easily applied in the diagonal direction than in the horizontal. Thus, referring back to the NAT-type materials where both rotation and distortion can occur, an on-axis stretch results in more resistance to rotation with an accompanying distortion of the rotating units. A stretching force applied at 45° results in less resistance to rotation, and in this case, rotation rather than distortion is the main deformational effect.

In contrast to the differing behavior of the square cross section with the direction of applied stress, the absolute changes in hinge angle with applied stress in fact show little difference (Supporting Information). There is no evidence that the rotational effect is more pronounced for an off-axis stretch compared to an on-axis stretch: it is the degree of chain distortion that actually changes with direction of applied stress.

Conclusions

By "off-axis analysis" of experimental and simulated elastic constants for natrolite we have shown that the Poisson's ratios ν_{xy} and ν_{yx} would be negative if the zeolite material were to be subjected to stress at 45° to either the *x* or *y* crystallographic axes. This is the first example of auxetic behavior in a zeolite material, and this result for natrolite adds to the small number of inorganic network structures that are now known to possess negative Poisson's ratios, which includes α-cristobalite, which has an aggregate negative Poisson's ratio,[7] and paratellurite, α-TeO_2, which shows an off-axis Poisson's ratio ν_{xy} at 45° rotation about *z*.[43] Furthermore, we predict similar behaviors for four other members of the NAT family.

Using two distinct approaches to simulation (a force-field method and the molecular dynamics method of Parrinello and Rahman), we propose that the simple "rotating squares" model originally proposed as a model for predicted negative Poisson's ratio in NAT materials, and which gives a value of $\nu_{xy} = \nu_{yx} = -1$ at all directions of applied stress,[24] is modified by the presence of extraframework cations and water molecules such that the square units deform due to rotation of tetrahedral units within the chain, as well as rotating about their hinges. Such a deformation has in fact previously been seen using crystallography, where ion exchange of sodium for lithium in natrolite results in only a small change of Pauling angle, the main deformation being a distortion of the chain with a resulting smaller chain cross section.[44] Our simulations are thus producing a chemically valid structural deformation.

For a hypothetical siliceous natrolite where extraframework cations and water molecules are absent,[17] a negative Poisson's ratio in the *xy* plane is predicted at all orientations of applied stress about *z*. Our studies show however that for "real" zeolites where cations and water molecules are present within the pores, the Poisson's ratio is not always negative in this plane. It can be envisaged that the interstitial species present physically or electronically restrict rotation of framework units. In this case, the deformation behavior can no longer be described in terms of a simple rotational model but account has to be taken of distortion of the rotating units on stretching; i.e., these units are not rigid but deform to some extent and the direction of applied stress determines to what extent the units will rotate or distort. An off-axis stress applied at 45° to the crystallographic *x* or *y* axes causes less distortion of the rotating units and rotation of the square cross-section chains is then the dominant effect, resulting in a negative Poisson's ratio for the NAT zeolites. It appears to be the total volume of extraframework species that dictates the balance of the distortion vs rotation: natrolite, $Na_2[Al_2$-

(42) Goryainov, S. V. *Eur. J. Mineral.* **2005**, *17*, 201.

(43) Ogi, H.; Fukunaga, M.; Hirao, M.; Ledbetter, H. *Phys. Rev. B* **2004**, *69*, 024104.

(44) Baur, W. H.; Kassner, D.; Kim, C. H.; Sieber, N. H. W. *Eur. J. Mineral.* **1990**, *2*, 761.

$Si_3O_{10}]\cdot 2H_2O$, mesolite, $Na_{0.67}Ca_{0.67}[Al_2Si_3O_{10}]\cdot 2.67H_2O$, and scolecite, $Ca[Al_2Si_3O_{10}]\cdot 3H_2O$, all have similar predicted elastic moduli, and Poisson's ratios, whereas in metanatrolite, $Na_2[Al_2Si_3O_{10}]$, and ammonium-exchanged natrolite, $(NH_4)_2[Al_2Si_3O_{10}]$, both with fewer extraframework species, the rotational effect is more dominant, resulting in lower elastic moduli and larger extremes of Poisson's ratios.

Acknowledgment. We thank the EPSRC for funding this work and for the provision of a DTA studentship to J.J.W.

Supporting Information Available: Tables S1−S4; Figures S4 and S5. This material is available free of charge via the Internet at http://pubs.acs.org.

CM062473W